



# Biomass burning influences determination based on PM<sub>2.5</sub> chemical composition combined with fire counts at southeastern Tibetan Plateau during pre-monsoon period



Ningning Zhang<sup>a,b,\*</sup>, Junji Cao<sup>a,b,c</sup>, Qiyuan Wang<sup>a,b</sup>, Rujin Huang<sup>a,b,d</sup>, Chongshu Zhu<sup>a,b</sup>, Shun Xiao<sup>e</sup>, Linlin Wang<sup>f</sup>

<sup>a</sup> Key Laboratory of Aerosol Chemistry and Physics, Institute of Earth Environment, Chinese Academy of Sciences, Xi'an 710061, China

<sup>b</sup> SKLLQG, Institute of Earth Environment, Chinese Academy of Sciences, Xi'an, China

<sup>c</sup> Institute of Global Environmental Change, Xi'an Jiaotong University, Xi'an, China

<sup>d</sup> Lab of Atmospheric Chemistry, Paul Scherrer Institute (PSI), 5232 Villigen, Switzerland

<sup>e</sup> School of Geography and Tourism, Shaanxi Normal University, Xi'an 710062, China

<sup>f</sup> College of Architectural Engineering, Binzhou University, Binzhou 256600, China

## ARTICLE INFO

### Keywords:

Biomass burning

Fire counts

Chemical composition

Aerosols

Mt. Yulong

## ABSTRACT

Influences of biomass burning (BB) on a high altitude site were investigated by collecting fine particulate matter (PM<sub>2.5</sub>) samples from 29 March to 27 April of 2012 at Mt. Yulong (4500 m above sea level), and analyzing them for selected chemical species including water soluble ions (WSIs), organic carbon (OC), elemental carbon (EC), polycyclic aromatic hydrocarbons (PAHs) and *n*-alkanes. The mean PM<sub>2.5</sub> mass loading for the study was  $6.30 \pm 4.90 \mu\text{g m}^{-3}$ , and  $15.48 \pm 2.82 \mu\text{g m}^{-3}$  and  $1.75 \pm 0.41 \mu\text{g m}^{-3}$  for a high and a low PM episode, respectively. WSIs accounted for 62% of the total mass, and  $\text{SO}_4^{2-}$  was the dominant anion and  $\text{NH}_4^+$  was the main cation. PAHs were mainly 3 ring compounds, fluorene (Flo) and phenanthrene (Phe) together accounted for 54% of the total PAHs. For *n*-alkanes, *n*-Nonacosane (C<sub>29</sub>) concentration was the highest with the value of  $1.09 \pm 1.18 \text{ ng m}^{-3}$ , following is *n*-Hentriacontane (C<sub>31</sub>) and *n*-Heptacosane (C<sub>27</sub>) suggested that *n*-alkane in our samples were mainly contributed by biogenic sources. BB emission was confirmed by the diagnostic ratios, and it also had a significant influence on aerosol optical depth (AOD) distribution and enhances the concentration of most species, especially for OC, K<sup>+</sup> and EC. Significant relationships were found between daily fire counts and BB species, and correlation coefficients (*r*) for mass, K<sup>+</sup>, OC, and EC were 0.58, 0.57, 0.53 and 0.60 (*n* = 29, *P* < 0.01), respectively. It indicated that daily fire counts can advance our understanding of how biomass burning affect aerosols and air quality at a high-altitude site.

## 1. Introduction

Biomass burning (BB) is a global phenomenon, and emissions from the fires are an important source for atmospheric trace gases and particulate matter (PM) that can impact the environment and climate (Crutzen et al., 1979; Andreae, 1983; Crutzen and Andreae, 1990; Lin et al., 2013; Khamkaew et al., 2016; Yadav et al., 2017; Vicente and Alves, 2017). In recent decades, increased attention has been focused on BB and the physical, chemical, and thermodynamic properties of gases and PM emitted by the fires (Reid et al., 2005; Niu et al., 2016; Souza et al., 2016). Much of the interest in BB has grown out of its impacts on ecology, human health, climate, cloud condensation nuclei (CCN), and so on (Reid et al., 2005; Lin et al., 2016; Pani et al., 2016;

Alves et al., 2017). Natural forest fires and anthropogenic burning in South and Southeast (S/SE) Asia make these the two major BB source regions in the world, and emissions there are especially strong during the pre-monsoon period (Haberle et al., 2001; Pochanart et al., 2003; Radojevic, 2003; Sheesley et al., 2003; Venkataraman et al., 2005; Chang and Song, 2010; Ram and Sarin, 2010; Zhao et al., 2013). Smoke from these regions has been shown to be transported to Tibetan Plateau (TP), Eastern Asia, the Indian Ocean, the western Pacific Ocean (Ma et al., 2003; Wang et al., 2007; Huang et al., 2013; Sang et al., 2013), and it can travel as far as Europe in the upper troposphere (Stohl et al., 2007).

The chemical composition of atmospheric particles has been studied extensively to evaluate the sources for aerosol particles and the

\* Corresponding author at: Key Laboratory of Aerosol Chemistry and Physics, Institute of Earth Environment, Chinese Academy of Sciences, Xi'an 710061, China  
E-mail address: [zhangnn@ieecas.cn](mailto:zhangnn@ieecas.cn) (N. Zhang).

influences of BB on regional environments in S/SE Asia. For example, studies conducted for the Indian Ocean Experiment (INDOEX) (Ramanathan et al., 2007; Gustafsson et al., 2009; Stone et al., 2007) and 7 South East Asian Studies (7 SEAS) (Lin et al., 2013 and references in that special issue). Other field studies of BB emissions have been conducted in urban areas (C.S. Zhu et al., 2017; J. Zhu et al., 2017), rural areas (Sang et al., 2013), at a high altitude (> 4000 m) site (Decesari et al., 2010), and some have involved highly time-resolved in-situ measurements (Zheng et al., 2017). Analyses of the temporal and spatial variations of particle and gas chemistry for above studies have confirmed that BB emissions from S/SE Asia can significantly influence regional or global atmospheric chemistry.

Fire counts made with satellites have been proven as a useful tool for studying BB emissions (Kaufman et al., 1998; Giglio et al., 2013; Sayer et al., 2016; Tsay et al., 2016; Pimonsree et al., 2017). The broad spatial coverage of satellite has enabled researchers to use fire counts as constraints on bottom-up fire emission inventories (Soja et al., 2009; Zeng et al., 2016). Zeng et al. (2016) combined Moderate Resolution Imaging Spectrometer (MODIS) fire counts and a bottom-up approach to develop a hybrid emission inventory for the southeastern United States. The inventory developed from that study improved the performance of the Community Multiscale Air Quality (CMAQ) model, especially for organic carbon (OC), elemental carbon (EC), and PM<sub>2.5</sub>. Schultz (2002) characterized the seasonal and interannual variability of emissions from vegetation fires using the Along-Track Scanning Radiometer (ATSR) sensor on the European Remote-Sensing satellite (ERS-2). It can be concluded that studies of fire counts clearly have the potential to improve BB emission inventories and simulations of regional atmospheric models, particularly for remote regions where fire activity records are spotty. However, the relationship between fire counts and the chemical characteristic of aerosol should be evaluated firstly. It has been reported that monthly fire counts have a significant relationship with chemical components over the southeastern United States, such as K<sup>+</sup> and levoglucosan which originate from BB (Zeng et al., 2008; Zhang et al., 2010), and there have been relatively few studies that have connected the information on daily fire counts with chemical data, especially at remote area.

For our study, PM<sub>2.5</sub> samples were collected at Mt. Yulong during the pre-monsoon period, and the concentrations of selected species, including WSIs, OC, EC, PAHs and *n*-alkanes, were determined to investigate the influences of BB on the ambient aerosol. We also used data obtained from MODIS to investigate possible relationships between the daily fire counts and chemical species concentrations.

## 2. Methods

### 2.1. Sampling site

Mt. Yulong is located in the Hengduan Mountain Range on the southeastern Tibetan Plateau, 25 km north of Lijiang city, Yunnan Province, southwest China. The altitude of the peak is 5596 m above sea level (asl-all elevations that follow are asl). Mt. Yulong has become a tourist destination because of its temperate glaciers and the beautiful scenery, and the number of tourists who visited the area approached 3 million in 2012. According to our investigation, in the main tourist area, gasoline and diesel burning vehicles can only drive as far as the Ganhaizi Basin (3100 m), and from there tourists are transported by green buses and electric vehicles to a station at 3356 m. The visitors are finally transferred to the glacier area at 4500 m by means of a ropeway. The sampling site itself (27.10N, 100.20E) was at an elevation of ~4500 m, about 200 m from the ropeway station (Fig. 1). The area around the sampling site is open, and there are no obvious sources for anthropogenic emissions nearby.

### 2.2. Meteorology

The climate of southwestern China, including Mt. Yulong, can be divided into the monsoon (May to October) and non-monsoon (November to April in the following year) periods. These conditions are driven by the southwestern monsoon circulation and the southern branch of the westerly circulation. The non-monsoon period can be subdivided into a post-monsoon period (November to January next year) and a pre-monsoon period (February to April), which is when our study was conducted. Meteorological data obtained from an automatic weather station near the sampling site are presented in Fig. 2. During the sampling period, the temperature was most often < 0 °C and ranged from -6.0 °C to 5.8 °C; the mean relative humidity (RH) was 66.4% ± 22%, and wind speed was 6.0 ± 3.8 m s<sup>-1</sup>. Although the winds were predominantly westerly during our study, the near surface wind flow can be strongly influenced by the local topography.

### 2.3. Sampling and chemical analysis

PM<sub>2.5</sub> samples were collected 2 m above ground level from 29 March to 27 April 2012. Quartz filters (2 μm pore size, 37 mm diameter, Whatman Plc, Little Chalfont, UK) were used as the sampling substrates. The sampler (URG-3000 N, URG Corp., Chapel Hill, NC, USA) was powered by 220 V alternating current. The volume of air sampled was measured with an in-line flow meter, and the mean flow rate was 22 L/min. Corrections for ambient temperature and pressure allowed conversion of the measured volumes to standard cubic meters.

All filters were pre-combusted at 800 °C for 3 h, and then conditioned at 50% RH and 25 °C for over 24 h in preparation for gravimetric analysis. A Sartorius MC5 electronic microbalance (Sartorius, Göttingen, Germany) with a sensitivity of 1 μg was used for weighting filters. After sampling, filters were again conditioned and re-weighed to obtain the accumulated masses needed to calculate the mass concentrations. The filters were then cut into portions for chemical analysis. Blank filters were handled in the same manner as the samples.

One or two punches (0.526 cm<sup>2</sup>) of each filter was used for the determination of carbon fractions (OC and EC) with the use of a DRI Model 2001 Thermal/optical Carbon Analyzer following the Interagency Monitoring of Protected Visual Environments (IMPROVE-A) thermal/optical reflectance protocol (Cao et al., 2007). Char-EC and soot-EC were calculated by the method of Han et al. (2007). Two or three punches from each filter were analyzed for PAHs and *n*-alkanes using a thermal desorption-gas chromatography/mass spectrometry method with an Agilent GC 7890A/MS 5975C system (Agilent Technologies, Santa Clara, CA, USA; Ho et al., 2011). The remainder of the filter was used for determination of WSIs (SO<sub>4</sub><sup>2-</sup>, NO<sub>3</sub><sup>-</sup>, Cl<sup>-</sup>, NH<sub>4</sub><sup>+</sup>, Na<sup>+</sup>, K<sup>+</sup>, Ca<sup>2+</sup>, Mg<sup>2+</sup>) (Shen et al., 2009) by an ion chromatography procedure (IC, Dionex 500, Dionex Corp, Sunnyvale, CA., USA).

### 2.4. Satellite data

In this study, MODIS products were used for calculating aerosol optical depths (AOD), and they obtained from the website of <http://disc.sci.gsfc.nasa.gov/giovanni/overview/index.html>. The distributions of fire counts were obtained from <https://firms.modaps.eosdis.nasa.gov/firemap/>. Achieve files of fire counts were downloaded from the Global Fire Emissions Database, Version 4 ([https://daac.ornl.gov/cgi-bin/dsvviewer.pl?ds\\_id=1293](https://daac.ornl.gov/cgi-bin/dsvviewer.pl?ds_id=1293)). Fire counts with confidence levels > 20 were selected for our analyses.

### 2.5. Backward trajectories

Backward trajectories were obtained using the hybrid single-particle Lagrangian integrated trajectory (HYSPLIT-4) model (<http://www.arl.noaa.gov/ready/hysplit4.html>) to trace the air masses. The end location was set at our sampling sites running for 72 h with heights of 100 m

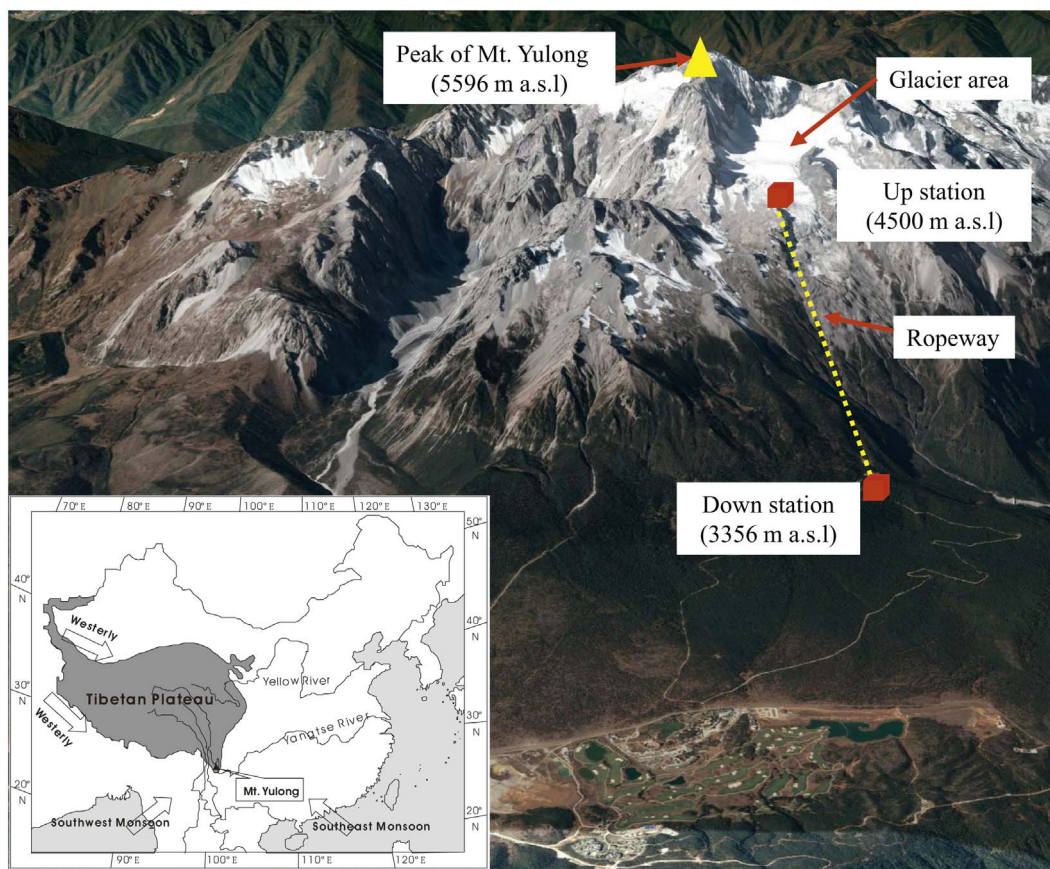


Fig. 1. Location of the Mt. Yulong sampling site (asl means above sea level).

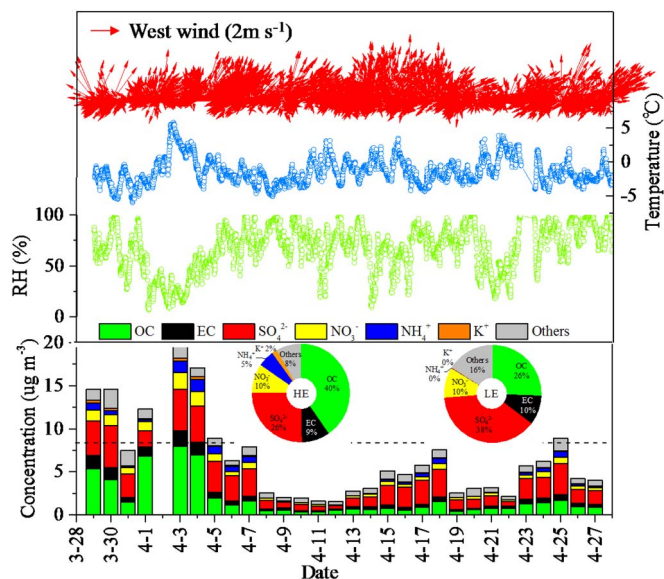


Fig. 2. Variations of meteorological parameters and the chemical composition during the sampling time. HE and LE stand for high and low particulate matter episodes, respectively (dashed line represents average mass concentration).

above ground level, and the ending time was 12:00 (04:00 UTC (Coordinated Universal Time)) of Beijing time.

### 3. Results and discussion

#### 3.1. Mass variations and particulate matter episodes

The PM<sub>2.5</sub> mass concentrations (sum of WSIs, OC, EC, PAHs and *n*-alkanes) and their daily variations are shown in Fig. 2. The mass loadings during the study ranged from 1.38 to 19.53 µg m<sup>-3</sup>, and the

Table 1  
Concentrations of selected chemical components (µg m<sup>-3</sup>) in aerosol particles from Mt. Yulong.

| Species                              | All samples |      | High PM episode |      | Low PM episode |      | H/L    |
|--------------------------------------|-------------|------|-----------------|------|----------------|------|--------|
|                                      | Mean        | SD   | Mean            | SD   | Mean           | SD   |        |
| Total mass                           | 6.30        | 4.90 | 15.48           | 2.82 | 1.75           | 0.41 | 8.83   |
| TC                                   | 2.39        | 2.60 | 7.69            | 1.63 | 0.62           | 0.12 | 12.39  |
| OC                                   | 1.84        | 2.17 | 6.24            | 1.51 | 0.45           | 0.10 | 13.89  |
| EC                                   | 0.55        | 0.46 | 1.45            | 0.30 | 0.17           | 0.04 | 8.47   |
| Cl <sup>-</sup>                      | 0.11        | 0.06 | 0.12            | 0.03 | 0.10           | 0.02 | 1.28   |
| NO <sub>3</sub> <sup>-</sup>         | 0.60        | 0.47 | 1.46            | 0.34 | 0.18           | 0.07 | 8.30   |
| SO <sub>4</sub> <sup>2-</sup>        | 2.20        | 1.33 | 3.94            | 1.20 | 0.68           | 0.24 | 5.84   |
| Na <sup>+</sup>                      | 0.20        | 0.11 | 0.21            | 0.12 | 0.08           | 0.05 | 2.67   |
| NH <sub>4</sub> <sup>+</sup>         | 0.41        | 0.41 | 0.84            | 0.55 | 0.00           | 0.00 | 288.45 |
| K <sup>+</sup>                       | 0.10        | 0.10 | 0.27            | 0.08 | 0.00           | 0.00 | 76.48  |
| Mg <sup>2+</sup>                     | 0.03        | 0.03 | 0.07            | 0.02 | 0.01           | 0.01 | 6.89   |
| Ca <sup>2+</sup>                     | 0.35        | 0.30 | 0.84            | 0.30 | 0.09           | 0.08 | 9.39   |
| Total PAHs <sup>a</sup>              | 0.97        | 0.59 | 1.74            | 0.74 | 0.41           | 0.19 | 4.21   |
| Total <i>n</i> -alkanes <sup>a</sup> | 6.53        | 5.98 | 16.70           | 7.68 | 2.80           | 1.92 | 5.98   |

<sup>a</sup> Indicates the units are ng/m<sup>3</sup>.

mean value was  $6.30 \pm 4.90 \mu\text{g m}^{-3}$  (Table 1). Compared with other  $\text{PM}_{2.5}$  mass concentrations monitored at rural site of TP, our results were lower than Qilian Shan which is located at the northern boundary of the TP, the annual mean  $\text{PM}_{2.5}$  mass concentration was  $9.5 \pm 5.4 \mu\text{g m}^{-3}$  (Xu et al., 2015); Qinghai Lake, located on north-eastern TP, the  $\text{PM}_{2.5}$  mass loading in summertime was  $21.27 \pm 10.70 \mu\text{g m}^{-3}$  (Zhang et al., 2014), and Tengchong Mountain site, located on the southeastern TP, the concentration from April to May was  $19.0 \pm 12.4 \mu\text{g m}^{-3}$  (Sang et al., 2013).

Relatively high mass concentrations were found at Yulong in late March and early April 2012, and on the five days with the highest  $\text{PM}_{2.5}$  mass (29 and 30 March, 1, 3, and 4 April), the average value was  $15.48 \pm 2.82 \mu\text{g m}^{-3}$ , and that is defined as a high PM episode (HE) period. The  $\text{PM}_{2.5}$  mass concentration decreased on 4 April and reached its lowest concentration from 8 to 12 April, which is considered a low PM episode (LE). In fact, the average mass concentration during the LE was  $1.75 \pm 0.41 \mu\text{g m}^{-3}$ , which is only about 11% of that during the HE. These results show that large fluctuations in daily  $\text{PM}_{2.5}$  mass levels occurred during the pre-monsoon period, and this is one reason why the standard deviations for the mass loadings during the pre-monsoon were higher than those found for the monsoon or post-monsoon in studies by Decesari et al. (2010), Zhao et al. (2013), and Zhang et al. (2016).

The relative abundances of the chemical species (OC, EC,  $\text{SO}_4^{2-}$ ,  $\text{NO}_3^-$ ,  $\text{NH}_4^+$ ,  $\text{K}^+$  and others (including PAHs, *n*-alkanes,  $\text{Na}^+$ ,  $\text{Ca}^{2+}$  and  $\text{Mg}^{2+}$ )) also differed between LE and HE periods (Fig. 2). During the HE period, OC was the dominant component of  $\text{PM}_{2.5}$ , accounting for 40% of the mass, and the two next most abundant species were  $\text{SO}_4^{2-}$  (26%) and  $\text{NO}_3^-$  (10%). In contrast, sulfate showed the highest percent contribution to the measured mass (38%) during the LE period, and even though OC was the second largest contributor to the mass during the LE (26%), it accounted for much smaller fraction of the mass than in the HE period. The high contributions of OC were also confirmed by the results for ultrafine particles during biomass burning period in rural area (C.S. Zhu et al., 2017; J. Zhu et al., 2017) and research of biomass burning emission factor (Tian et al., 2017).

### 3.2. Chemical composition

#### 3.2.1. Water soluble ions

The grand average sum of the measured WSIs was  $3.91 \pm 2.55 \mu\text{g m}^{-3}$ , and they accounted for 62% of the total mass. The most abundant anion in terms of mass was  $\text{SO}_4^{2-}$  while the dominant cation was  $\text{NH}_4^+$ , and the rest of the ion concentrations decreased in the order  $\text{NO}_3^- > \text{Ca}^{2+} > \text{Na}^+ > \text{Cl}^- > \text{K}^+ > \text{Mg}^{2+}$ . A significant correlation ( $r^2 = 0.95$ ,  $P < 0.001$ ) was found between the cation equivalent ( $\text{CE} = \text{Na}^+ / 23 + \text{NH}_4^+ / 18 + \text{K}^+ / 39 + \text{Mg}^{2+} / 12 + \text{Ca}^{2+} / 20$ ) and anion equivalent ( $\text{AE} = \text{SO}_4^{2-} / 48 + \text{NO}_3^- / 62 + \text{Cl}^- / 35.5$ ), and this indicates that the most important ions in terms of mass were measured on the filters. Meanwhile, the mean CE/AE ratio was 0.73 which appear to be related to undetected  $\text{H}^+$ .

All ions showed higher concentrations during the HE period than the LE period, and the mass ratios of HE/LE were 5.8, 8.3, 288.5, 9.4, 2.7, 1.3, 76.5 and 6.9 for  $\text{SO}_4^{2-}$ ,  $\text{NO}_3^-$ ,  $\text{NH}_4^+$ ,  $\text{Ca}^{2+}$ ,  $\text{Na}^+$ ,  $\text{Cl}^-$ ,  $\text{K}^+$  and  $\text{Mg}^{2+}$ , respectively. The concentrations of both  $\text{NH}_4^+$  and  $\text{K}^+$  were very low during LE period, often below their detect limits, and this suggests that their concentrations at that time may have approached background values. Those low values during the LE also indicate that the other sources for  $\text{K}^+$ , such as regional crustal dust were negligible, and this supports the argument that the main source for the  $\text{K}^+$  in our samples was BB. Low concentrations of  $\text{NH}_4^+$  and  $\text{K}^+$  have been previously reported for Lulang, which is located on the southeastern side of the TP (Zhao et al., 2013) and two other sites on the TP, Nepal (Decesari et al., 2010) and Qomolangma (Cong et al., 2015). Meanwhile, the correlation between  $\text{NH}_4^+$  and  $\text{K}^+$  was significant ( $r^2 = 0.81$ ,  $P < 0.001$ ,  $N = 29$ ), which implies that they were from related sources or transported together. Engling et al. (2011) and Cong et al. (2015)

also have reported that emissions from BB on the southern TP are rich in  $\text{NH}_4^+$  and  $\text{K}^+$ , and therefore a common BB source is indicated.

#### 3.2.2. Carbonaceous components

The mean concentration of OC was  $1.84 \pm 2.17 \mu\text{g m}^{-3}$ , which is close to  $2.4 \mu\text{g m}^{-3}$  of OC found in  $\text{PM}_{10}$  at NCO-P (Nepal, 5079 m) (Decesari et al., 2010), but lower than  $5.15 \mu\text{g m}^{-3}$  of OC in TSP at Lulang (Tibet, 3360 m) during the pre-monsoon (Zhao et al., 2013). Meanwhile, the mean EC concentration in our study ( $0.55 \pm 0.46 \mu\text{g m}^{-3}$ ) was close to the values of  $0.5 \mu\text{g m}^{-3}$  at NCO-P and  $0.84 \mu\text{g m}^{-3}$  at Lulang. The concentration of TC (total carbon, sum of OC and EC) was  $2.39 \pm 2.60 \mu\text{g m}^{-3}$  which accounted for 38% of the total mass. The ratio of TC/ $\Sigma$ WSIs (sum of  $\text{SO}_4^{2-}$ ,  $\text{NO}_3^-$ ,  $\text{NH}_4^+$ ,  $\text{Ca}^{2+}$ ,  $\text{Na}^+$ ,  $\text{Cl}^-$ ,  $\text{K}^+$  and  $\text{Mg}^{2+}$ ) at our site was 0.61 which is much lower than 1.57 at Lulang or 0.95 at NCO-P. The TC/ $\Sigma$ ions ratios were 0.55 and 0.99 during LE period and HE period, respectively, and therefore, relatively more carbonaceous aerosols were present during the HE period.

The concentrations of OC and EC were correlated significantly ( $r = 0.94$ ,  $P < 0.001$ ), indicating they had related sources or were transported to the site together. The overall average OC/EC ratio was 2.92, and even though this value is higher than what is typically found at urban sites (Cao et al., 2003), it is much lower than the values reported at some other high altitude sites on the TP. For example, some of the reported OC/EC ratios are 10 for TSP from Muatagh Ata (4500 m) (Cao et al., 2009), 4.8 for  $\text{PM}_{10}$  from the Himalayas (5079 m) (Decesari et al., 2010), and 4.77 for  $\text{PM}_{2.5}$  from Qinghai Lake (3200 m) (Zhang et al., 2014). On the other hand, an OC/EC ratio of 2.63, which is lower than at our site, was found for  $\text{PM}_{10}$  samples collected at Tengchong (1950 m) (Sang et al., 2013).

#### 3.2.3. PAHs and *n*-alkanes

The total concentrations of the measured PAHs ( $\Sigma$ PAHs) ranged from 0.20 to  $2.57 \text{ ng m}^{-3}$  with a mean value of  $0.97 \text{ ng m}^{-3}$ , and this is much lower than what has been reported for most urban sites, such as  $104 \pm 130 \text{ ng m}^{-3}$  in Beijing (Ma et al., 2011) or  $10 \pm 6.6 \text{ ng m}^{-3}$  in Lhasa (Liu et al., 2013). However, our  $\Sigma$ PAHs value was higher than at Lulang ( $0.59 \pm 0.52 \text{ ng m}^{-3}$ ) (Chen et al., 2014) or Mt. Halla ( $0.40 \pm 0.58 \text{ ng m}^{-3}$ ), a background location in South Korea (Lee et al., 2008). Fluorene (Flo) and phenanthrene (Phe) were the two most abundant PAHs (Table 2), with mean values of  $0.28 \pm 0.16 \text{ ng m}^{-3}$  and  $0.24 \pm 0.58 \text{ ng m}^{-3}$ , respectively, and together Flo and Phe accounted for 54% of  $\Sigma$ PAHs. It is noteworthy that the mean concentration of benzo[*a*]pyrene (BaP) during the campaign was  $0.03 \pm 0.03 \text{ ng m}^{-3}$ , and that level is well below the air-quality standard of  $2.5 \text{ ng m}^{-3}$  established by Ministry of Environmental Protection of China in 2012.

The average concentration of the total quantified *n*-alkanes ( $\Sigma$ *n*-alkanes) was  $6.53 \pm 5.98 \text{ ng m}^{-3}$ , which was much lower than typical urban levels, such as  $163.0 \pm 193.5 \text{ ng m}^{-3}$  in  $\text{PM}_{2.5}$  from Beijing (Huang et al., 2006),  $141\text{--}392 \text{ ng m}^{-3}$  in  $\text{PM}_{10}$  from Guangzhou (Bi et al., 2005), or  $31.0 \pm 296.8 \text{ ng m}^{-3}$  in TSP from Lhasa (Gong et al., 2011). On the other hand, our results are comparable with the values reported for rural areas, such as  $1.25 \pm 2.28 \text{ ng m}^{-3}$  at Lulang (Chen et al., 2014),  $7\text{--}95 \text{ ng m}^{-3}$  in Finland (Rissanen et al., 2006), and  $8.2 \text{ ng m}^{-3}$  in Sweden (Wingfors et al., 2011).

The carbon maximum number ( $C_{\text{max}}$ ) for all samples and the HE and LE groups of samples were  $C_{29}$  (Fig. 3), its mean concentration was  $1.09 \pm 1.18 \text{ ng m}^{-3}$ , and that was followed by  $C_{31}$  ( $0.78 \pm 0.90 \text{ ng m}^{-3}$ ). The high concentrations of these odd numbered carbon compounds suggest that the *n*-alkanes were mainly from higher plants. The values for the carbon preference index (CPI) ( $\text{CPI} = \Sigma(\text{C}_{19}\text{--}\text{C}_{35}) / \Sigma(\text{C}_{18}\text{--}\text{C}_{34})$ ) were  $2.08 \pm 0.48$ ,  $1.41 \pm 0.29$ ,  $2.67 \pm 0.29$ , for the entire sampling period, LE, and HE, respectively. All of these values were much greater than unity, which indicates the presence of terrestrial higher-plant waxes, which may have been in the

**Table 2**  
Concentrations (ng m<sup>-3</sup>) of polycyclic aromatic hydrocarbons (PAHs) and *n*-alkanes in PM<sub>2.5</sub> samples from Mt. Yulong.

| Compound                                       | Abbreviation (number of rings) | All samples |      | HE      |      | LE      |      |
|--|--------------------------------|-------------|------|---------|------|---------|------|
|  |                                | Average     | SD   | Average | SD   | Average | SD   |
| <b>Polycyclic aromatic hydrocarbons (PAHs)</b> |                                |             |      |         |      |         |      |
| Fluorene                                       | Flo (3 rings)                  | 0.28        | 0.16 | 0.42    | 0.21 | 0.15    | 0.09 |
| Phenanthrene                                   | Phe (3 rings)                  | 0.24        | 0.14 | 0.39    | 0.19 | 0.12    | 0.06 |
| Anthracene                                     | Ant (3 rings)                  | 0.04        | 0.02 | 0.07    | 0.04 | 0.02    | 0.01 |
| Fluoranthene                                   | Flu (4 rings)                  | 0.06        | 0.04 | 0.11    | 0.05 | 0.02    | 0.01 |
| Pyrene   | Pyr (4 rings)                  | 0.06        | 0.04 | 0.11    | 0.04 | 0.02    | 0.01 |
| Benzo[ <i>a</i> ]anthracene                    | BaA (4 rings)                  | 0.02        | 0.02 | 0.04    | 0.02 | 0.00    | 0.00 |
| Chrysene                                       | Chr (4 rings)                  | 0.04        | 0.04 | 0.11    | 0.06 | 0.01    | 0.00 |
| Benzo[ <i>b</i> ]fluoranthene                  | BbF (5 rings)                  | 0.04        | 0.03 | 0.10    | 0.03 | 0.01    | 0.01 |
| Benzo[ <i>k</i> ]fluoranthene                  | BkF (5 rings)                  | 0.04        | 0.03 | 0.08    | 0.03 | 0.01    | 0.00 |
| Benzo[ <i>a</i> ]fluoranthene                  | BaF (5 rings)                  | 0.01        | 0.01 | 0.01    | 0.01 | 0.00    | 0.00 |
| Benzo[ <i>e</i> ]pyrene                        | BeP (5 rings)                  | 0.04        | 0.03 | 0.08    | 0.03 | 0.01    | 0.00 |
| Benzo[ <i>a</i> ]pyrene                        | BaP (5 rings)                  | 0.03        | 0.03 | 0.07    | 0.03 | 0.01    | 0.00 |
| Perylene                                       | Per (5 rings)                  | 0.00        | 0.00 | 0.01    | 0.00 | 0.00    | 0.00 |
| Indeno[1,2,3- <i>cd</i> ]pyrene                | IcdP (6 rings)                 | 0.03        | 0.02 | 0.06    | 0.02 | 0.01    | 0.00 |
| Dibenzo[ <i>a,h</i> ]anthracene                | DahA (6 rings)                 | 0.00        | 0.00 | 0.01    | 0.00 | 0.00    | 0.00 |
| Benzo[ <i>ghi</i> ]perylene                    | BghiP (6 rings)                | 0.03        | 0.02 | 0.05    | 0.02 | 0.01    | 0.00 |
| Total PAHs                                     |                                | 0.97        | 0.59 | 1.74    | 0.74 | 0.41    | 0.19 |
| <b><i>n</i>-Alkanes</b>                        |                                |             |      |         |      |         |      |
| <i>n</i> -Heptadecane                          | C17                            | 0.57        | 0.37 | 0.99    | 0.37 | 0.23    | 0.14 |
| <i>n</i> -Octadecane                           | C18                            | 0.54        | 0.32 | 0.83    | 0.40 | 0.27    | 0.17 |
| <i>n</i> -Nonadecane                           | C19                            | 0.21        | 0.13 | 0.32    | 0.19 | 0.13    | 0.09 |
| <i>n</i> -Icosane                              | C20                            | 0.24        | 0.15 | 0.37    | 0.24 | 0.14    | 0.11 |
| <i>n</i> -Heneicosane                          | C21                            | 0.21        | 0.23 | 0.53    | 0.39 | 0.07    | 0.05 |
| <i>n</i> -Docosane                             | C22                            | 0.24        | 0.29 | 0.66    | 0.55 | 0.09    | 0.05 |
| <i>n</i> -Tricosane                            | C23                            | 0.35        | 0.42 | 1.04    | 0.69 | 0.12    | 0.06 |
| <i>n</i> -Tetracosane                          | C24                            | 0.25        | 0.26 | 0.66    | 0.42 | 0.12    | 0.07 |
| <i>n</i> -Pentacosane                          | C25                            | 0.34        | 0.35 | 0.95    | 0.47 | 0.17    | 0.13 |
| <i>n</i> -Hexacosane                           | C26                            | 0.23        | 0.21 | 0.58    | 0.25 | 0.19    | 0.17 |
| <i>n</i> -Heptacosane                          | C27                            | 0.50        | 0.52 | 1.42    | 0.63 | 0.26    | 0.21 |
| <i>n</i> -Octacosane                           | C28                            | 0.30        | 0.27 | 0.74    | 0.31 | 0.24    | 0.21 |
| <i>n</i> -Nonacosane                           | C29                            | 1.09        | 1.18 | 3.18    | 1.42 | 0.31    | 0.20 |
| <i>n</i> -Triacontane                          | C30                            | 0.24        | 0.23 | 0.63    | 0.28 | 0.16    | 0.13 |
| <i>n</i> -Hentriacontane                       | C31                            | 0.78        | 0.90 | 2.38    | 1.12 | 0.17    | 0.10 |
| <i>n</i> -Dotriacontane                        | C32                            | 0.12        | 0.13 | 0.35    | 0.17 | 0.06    | 0.05 |
| <i>n</i> -Tritriacontane                       | C33                            | 0.23        | 0.31 | 0.78    | 0.40 | 0.04    | 0.02 |
| <i>n</i> -Tetracontane                         | C34                            | 0.04        | 0.04 | 0.11    | 0.05 | 0.02    | 0.01 |
| <i>n</i> -Pentatriacontane                     | C35                            | 0.04        | 0.05 | 0.13    | 0.06 | 0.01    | 0.00 |
| <i>n</i> -Hexatriacontane                      | C36                            | 0.01        | 0.02 | 0.04    | 0.02 | 0.01    | 0.00 |
| Sum of <i>n</i> -alkanes                       |                                | 6.53        | 5.98 | 16.70   | 7.68 | 2.80    | 1.92 |

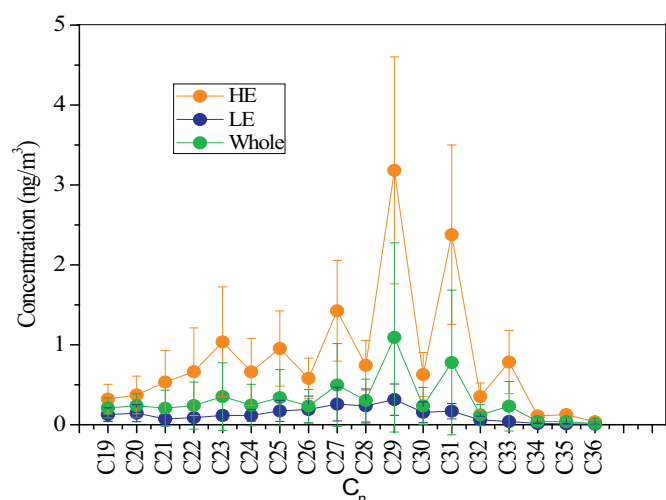


**Fig. 3.** Concentrations of *n*-alkanes in aerosol samples from Mt. Yulong from different periods. Whole stands for whole study; HE and LE as in Fig. 2.

BB emissions. Furthermore, a higher CPI was seen in the HE than in the LE, indicating a greater contribution of biogenic source materials during the heavy PM episode (Chen et al., 2014).

### 3.3. Diagnostic ratios and BB influences

The impact of BB on ambient aerosol samples can be evaluated by calculating and evaluating diagnostic ratios of chemical components (Table 3). The ratios of OC/EC, Char-EC/soot-EC, EC/TC and K<sup>+</sup>/EC have been applied to identify the possible sources (Cao et al., 2003; Han et al., 2009; Ram and Sarin, 2010; Zhang et al., 2014). PAH diagnostic ratios are also useful for distinguishing among fuel types and combustion sources (Ravindra et al., 2008) and in particular BB emissions (Yunker et al., 2002).

The mass ratio of OC/EC is one such tool commonly used for identifying PM from different fuel types—the principle behind this is that particles from BB have higher OC/EC ratios than those from fossil fuel combustion (Cao et al., 2003). At Mt. Yulong, the OC/EC ratios were 4.44, 2.82 and 2.92 for HE, LE, and the whole sampling period, but using this information for distinguishing sources has limitations. Char-EC/soot-EC ratios are influenced by fewer factors than OC/EC ratios (Han et al., 2007, 2009), and therefore this ratio has been proposed as a better indicator different fuel types than OC/EC. Char-EC/soot-EC ratios for BB typically exceed 10 (Chuang et al., 2014) and some of the reported values for BB emissions are 11.6 (Cao et al., 2005), 22.6 (Chow

**Table 3**  
Diagnostic chemical ratios for different periods.

| Ratio               | All samples |      | HE    |      | LE   |      | Reference value                                    |
|---------------------|-------------|------|-------|------|------|------|--|
|                     | Mean        | SD   | Mean  | SD   | Mean | SD   |  |
| OC/EC               | 2.92        | 1.07 | 4.44  | 1.43 | 2.82 | 1.24 |  |
| Char-EC/Soot-EC     | 8.88        | 4.65 | 14.94 | 7.60 | 6.12 | 3.01 |  |
| EC/TC               | 0.27        | 0.06 | 0.19  | 0.05 | 0.28 | 0.07 | 0.1–0.2, biomass burning; 0.6–0.7, fuel combustion |
| K <sup>+</sup> /EC  | 0.11        | 0.08 | 0.18  | 0.03 | 0.01 | 0.01 | 0.2–0.69, biomass burning                          |
| Flu/(Flu + Pyr)     | 0.53        | 0.03 | 0.52  | 0.01 | 0.57 | 0.02 | > 0.5, grass, wood, coal combustion                |
| IcdP/(IcdP + BghiP) | 0.51        | 0.03 | 0.54  | 0.04 | 0.49 | 0.01 | > 0.5, grass, wood, coal combustion                |

et al., 2004), and up to 31 (Chen et al., 2007). For coal combustion, char-EC/soot-EC is 1.9 (Cao et al., 2005); and for motor vehicle emissions the ratio is < 1 (Cao et al., 2005, 2006). As shown in Table 3, the char-EC/soot-EC ratios in our study were 14.94, 6.12 and 8.88 during the HE, LE and the entire study, respectively. This is strong evidence that BB emissions had significant influences on our samples, especially during the HE period. The ratios of EC/TC and K<sup>+</sup>/EC were also calculated (Table 3), and their characteristic values for BB emissions are 0.1–0.2 (Salam et al., 2003) and 0.2–0.69 (Ram and Sarin, 2010), respectively. At our site, the EC/TC and K<sup>+</sup>/EC ratios during the HE period were 0.19 and 0.18, respectively, and this is further supports our conclusion that the EC at that time was mainly from BB.

In this study, fluoranthene (Flu), pyrene (Pyr), benzo[e]pyrene (BeP), BaP, indeno[1,2,3-cd]pyrene (IcdP) and benzo[ghi]perylene (BghiP) were selected for calculating ratios. The Flu/(Flu + Pyr) and IcdP/(IcdP + BghiP) ratios indicate that the PAHs in our samples were mostly derived from wood, coal, and grass burning (Fig. 4). Coal burning is limited in southwest China, and therefore, it likely that BB is the major contributor to the PAHs. Indeed, the Flu/(Flu + Pyr) ratios for both the HE and LE plotted in the BB emission quadrant of Fig. 4 while most of the IcdP/(IcdP + BghiP) ratios for the LE were in the petroleum combustion quadrant. From these results, we conclude that BB was the main source for the PM<sub>2.5</sub> pollution during the HE, but during the cleaner conditions of the LE, both BB emissions and those from other anthropogenic sources impacted the samples.

A BaP/(BaP + BeP) ratio > 0.5 is characteristic of fresh particles while ratios < 0.5 are indicative of particle aging (Oliveira et al., 2011). The mean BaP/(BaP + BeP) ratios for our samples were 0.43, 0.37, and 0.46 for all samples, LE, and HE, respectively. Therefore, the

particles collected during the HE period evidently were relatively fresh, which means that the BB particles were probably transported to the site soon after they were emitted. Back trajectories shown that air mass transport straightly from the selected region (blue rectangle in Fig. 5) where labeled as intense fire counts during the HE period except on 4 April. In contrast, the air masses during the LE period rotated over northeastern Burma except on 11 April (Fig. 5). These trajectories support our contention that BB emissions were rapidly transported to Mt. Yulong from source regions during the HE period.

By comparing the distributions of fire sites and AOD, the influences from biomass burning on the atmosphere can be directly visualized, and the conditions for the HE and LE contrasted in Fig. 5. Broad areas of high AOD appeared over Southeast Asia during the HE period, and this was consistent with the distribution of fire counts, which means that the high AOD values almost certainly resulted from BB (Wang et al., 2015; C.S. Zhu et al., 2017; J. Zhu et al., 2017). The chemical composition of PM<sub>2.5</sub> was also obviously influenced by BB emissions, and this was made evident by the HE/average, LE/average and HE/LE mass ratios calculated for selected chemical species (Fig. 6). Indeed, the main species enhanced by BB emissions were OC, K<sup>+</sup> and EC, and their HE/average values were 3.39, 2.85 and 2.66, respectively. K<sup>+</sup> is richen in burning emissions from leaves, branches and grass (Ordou and Agranovski, 2017) and commonly used as an indicator of BB emissions (Andreae, 1983). Related studies by Zeng et al. (2008) and Sánchez et al. (2018) have also shown that the OC and EC concentrations can be enriched by BB emissions over the southeastern United States and Southwest Europe, respectively.

#### 3.4. Relationships between fire counts and chemistry

Monthly fire counts in the southeastern US were shown to be interrelated to emission inventories (Zeng et al., 2008), and a hybrid emission inventory combined with fire counts and a bottom-up inventory was later developed to enhance the performance of a community multi-scale air quality model (Zeng et al., 2016). Monthly fire counts were correlated significantly with the monthly concentrations of levoglucosan and water-soluble K<sup>+</sup> conducted in the southeastern US (Zhang et al., 2010). The implication of these results is that fire counts with monthly time resolution have the potential to improve our understanding of BB emissions.

Pollutant transport involves complex processes, however, and we investigated relationships between fire counts and species concentrations using our daily data as a case study. To evaluate this relationship, daily fire counts were collected for the region upwind of Mt. Yulong (88–98.5°E; 21.5–28°N) that includes northeast India and Burma (Fig. 5) and that has been shown to be the largest contributor to BB AOD over southwest China (C.S. Zhu et al., 2017; J. Zhu et al., 2017). Meanwhile, there is lower cloud cover in March over Burma (Sayer et al., 2016). The period from 29 March to 4 April showed numerous fire counts, and peak values of mass, K<sup>+</sup>, OC, and EC also occurred at this time. On 18 and 25 April, there were two small peaks in fire counts and two small corresponding peaks in mass, K<sup>+</sup>, OC, and EC (Fig. 7). The fire counts, aerosol masses, K<sup>+</sup>, OC, and EC all co-varied for these

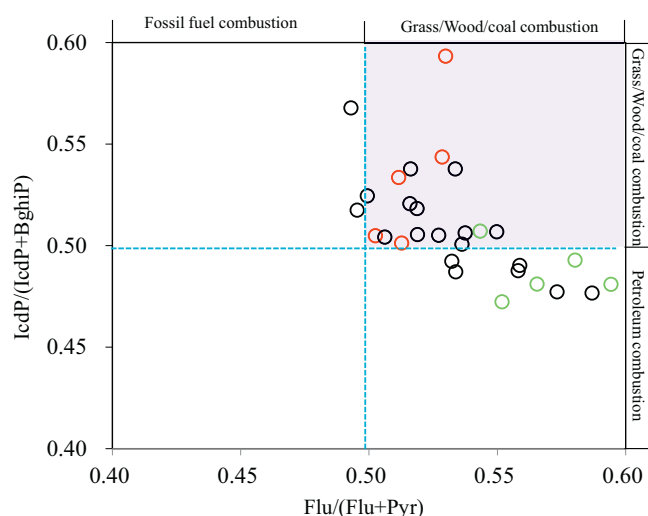


**Fig. 4.** Diagnostic ratios of Flu/(Flu + Pyr) vs. IcdP/(IcdP + BghiP) for different periods (red circles for the HE period, green circles for the LE period, and black circles for the other days). (For interpretation of the references to color in this figure legend, the reader is referred to the web version of this article.)

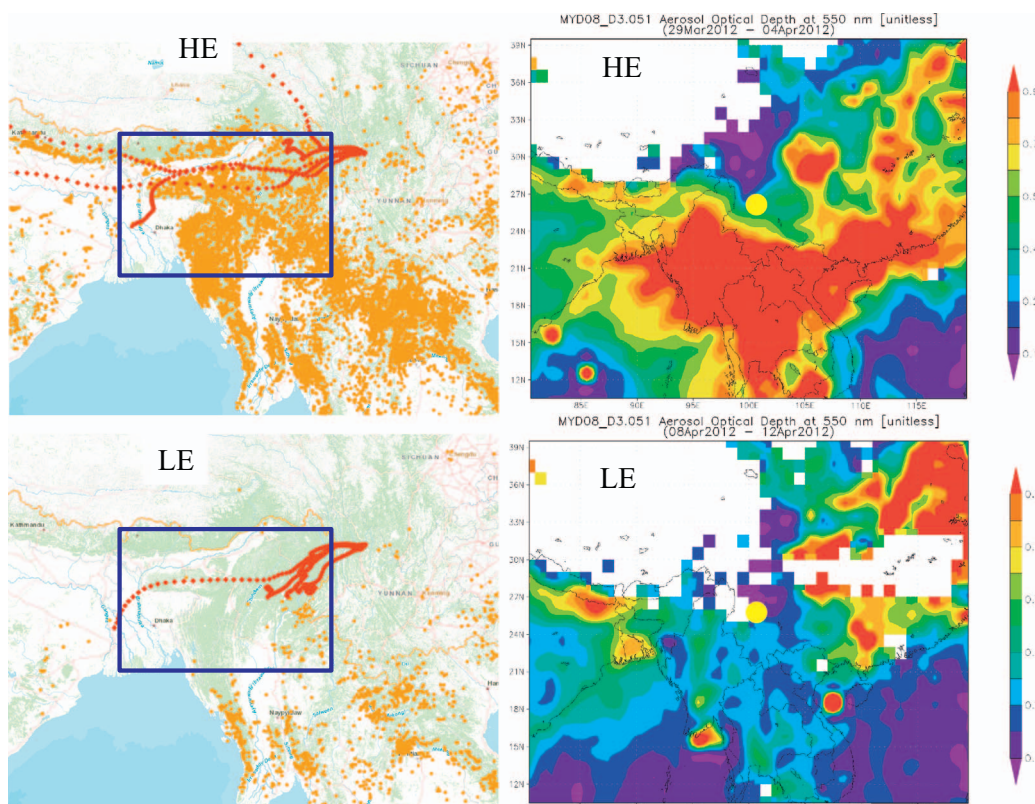


Fig. 5. Left panels: Distributions of fire counts (orange dots) and 72 h backward trajectories (red dotted lines) of days during HE and LE period, blue rectangles show the region selected for calculate fire counts; right panels: AOD distribution during HE and LE period obtained from MODIS (yellow dot marks the sampling site). (For interpretation of the references to color in this figure legend, the reader is referred to the web version of this article.)

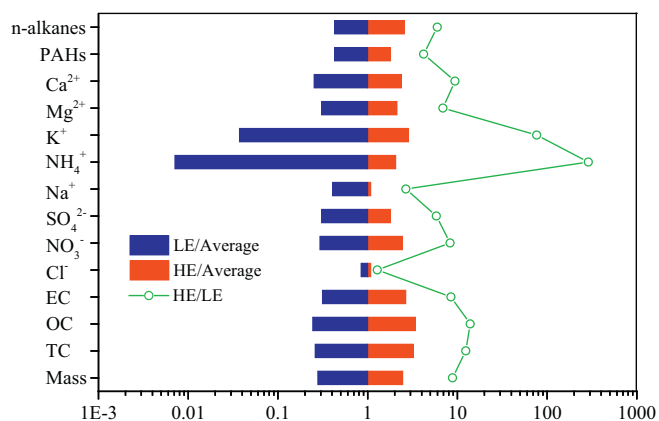


Fig. 6. Ratios of chemical concentrations for high and low particulate matter episodes to average (HE/average (red column) and LE/average (blue column), respectively) and HE/LE (green line). (For interpretation of the references to color in this figure legend, the reader is referred to the web version of this article.)

cases, and the correlation coefficients between fire counts and PM<sub>2.5</sub> mass, K<sup>+</sup>, OC, and EC were 0.58, 0.57, 0.53 and 0.60 (n = 29, P < 0.01), respectively. From this, we conclude that the daily fire counts were connected not only with the aerosol mass concentrations at Yulong but also with the loadings of chemical species associated with biomass burning. These relationships are likely related to the intensive fires that drive large fluctuations in aerosol species (Fig. 7) during the pre-monsoon period. More generally, our results suggest that daily fire counts also reflect the regional BB emissions during the pre-monsoon, and this may be helpful for improving regional atmospheric models.

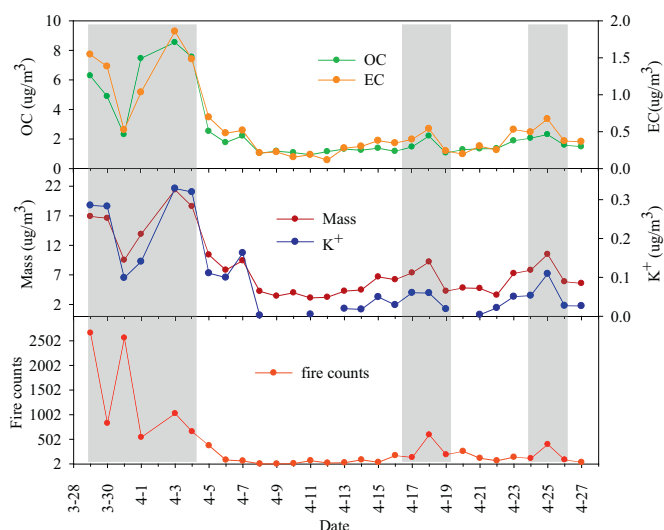


Fig. 7. Time series plots of fire counts, mass, K<sup>+</sup>, OC and EC (gray column represents the peak value).

#### 4. Conclusions

1. The arithmetic mean PM<sub>2.5</sub> mass concentrations were 6.30 μg m<sup>-3</sup>, 15.48 μg m<sup>-3</sup> and 1.75 μg m<sup>-3</sup> for the whole sampling period and HE and LE periods respectively, this illustrates the large fluctuations of daily PM<sub>2.5</sub> mass levels during the pre-monsoon. During the HE period, OC accounted for 40% of the mass, and that was followed by sulfate (26%); however, the relative abundances of these two species switched order during LE period when sulfate accounted for 38% and OC 26% of the mass. These results show that the aerosol

- chemical composition differed dramatically between high and low PM episodes in the pre-monsoon period.
- $\text{SO}_4^{2-}$  was the dominant anion in terms of mass and  $\text{NH}_4^+$  was the main cation. The concentrations of OC and EC were  $1.84 \pm 2.17 \mu\text{g m}^{-3}$  and  $0.55 \pm 0.46 \mu\text{g m}^{-3}$ , and the average OC/EC ratio was 2.92. The concentration of total PAHs was  $0.97 \text{ ng m}^{-3}$ ;  $\text{C}_{29}$  was the most abundant of the *n*-alkanes, with the concentration of  $1.09 \pm 1.18 \text{ ng m}^{-3}$ , and that was followed by  $\text{C}_{31}$  whose concentration was  $0.78 \pm 0.90 \text{ ng m}^{-3}$ . High concentrations of  $\text{NH}_4^+$  and  $\text{K}^+$ , the PAHs (Flo and Phe), and *n*-alkanes during the HE all point to influences from BB emissions.
  - Diagnostic ratios, including OC/EC, char-EC/soot-EC, EC/TC,  $\text{K}^+/\text{EC}$ , Fla/(Fla + Pyr), IcdP/(IcdP + BghiP) and BaP/(BaP + BeP), provided addition evidence that the samples from Mt. Yulong were influenced by BB emissions, especially during the HE period. Additionally, BB had an obvious influence on AOD, and it raised the concentrations of most species-the HE/average values for OC,  $\text{K}^+$  and EC were 3.39, 2.85 and 2.66, respectively.
  - A significant relationship between fire counts and aerosol species was found, and the correlation coefficients (*r*) between daily fire counts and mass,  $\text{K}^+$ , OC, and EC were 0.58, 0.57, 0.53 and 0.60 (*n* = 29, *P* < 0.01), respectively. Connecting fire counts with daily chemical data has increased our understanding of the impacts of biomass burning on the Tibetan Plateau, and this approach could lead to improvements in regional simulations.

## Acknowledgments

This work was supported by the Natural Science Foundation of China (NSFC 41673125, 40801028), the West Light Foundation of Chinese Academy of Sciences and the Major Research and Development Plan of Shandong Province (2015GSF117032). We sincerely thank the staffs at the Yulong Snow Mountain glacial and environment observation station who were instrumental in the field work.

## References

- Alves, N.D.O., Vessoni, A.T., Quinet, A., Fortunato, R.S., Kajitani, G.S., Peixoto, M.S., et al., 2017. Biomass burning in the Amazon region causes DNA damage and cell death in human lung cells. *Sci. Rep.* 7 (1).
- Andreae, M.O., 1983. Soot carbon and excess fine potassium: long-range transport of combustion-derived aerosols. *Science* 220, 1148–1151.
- Bi, X., Sheng, G., Peng, P., Chen, Y., Fu, J., 2005. Size distribution of *n*-alkanes and polycyclic aromatic hydrocarbons (PAHs) in urban and rural atmospheres of Guangzhou, China. *Atmos. Environ.* 39, 477–487.
- Cao, J.J., Lee, S.C., Ho, K.F., Zhang, X.Y., Zou, S.C., Fung, K.K., Chow, J.C., Watson, J.G., 2003. Characteristics of carbonaceous aerosol in Pearl River Delta region, China during 2001 winter period. *Atmos. Environ.* 37, 1451–1460.
- Cao, J.J., Wu, F., Chow, J.C., Lee, S.C., Li, Y., Chen, S.W., An, Z.S., Fung, K., Watson, J.G., Zhu, C.S., Liu, S.X., 2005. Characterization and source apportionment of atmospheric organic and elemental carbon during fall and winter of 2003 in Xi'an, China. *Atmos. Chem. Phys.* 5, 3127–3137.
- Cao, J.J., Lee, S.C., Ho, K.F., Fung, K., Chow, J.C., Watson, J.G., 2006. Characterization of roadside fine particulate carbon and its eight fractions in Hong Kong. *Aerosol Air Qual. Res.* 6, 106–122.
- Cao, J.J., Lee, S.C., Chow, J.C., Watson, J.G., Ho, K.F., Zhang, R.J., Jin, Z.D., Shen, Z.X., Chen, G.C., Kang, Y.M., Zou, S.C., Zhang, L.Z., Qi, S.H., Dai, M.H., Cheng, Y., Hu, K., 2007. Spatial and seasonal distributions of carbonaceous aerosols over China. *J. Geophys. Res.* 112, D22S11.
- Cao, J.J., Xu, B.Q., He, J.Q., Lin, X.Q., Han, Y.M., Wang, G.H., Zhu, C.S., 2009. Concentrations, seasonal variations, and transport of carbonaceous aerosols at a remote mountainous region in western China. *Atmos. Environ.* 43, 4444–4452.
- Chang, D., Song, Y., 2010. Estimates of biomass burning emissions in tropical Asia based on satellite-derived data. *Atmos. Chem. Phys.* 10 (5), 2335–2351.
- Chen, L.W.A., Moosmuller, H., Arnott, W.P., Chow, J.C., Watson, J.G., Susott, R.A., Babbitt, R.E., Wold, C.E., Lincoln, E.N., Hao, W.M., 2007. Emissions from laboratory combustion of wildland fuels: emission factors and source profiles. *Environ. Sci. Technol.* 41, 4317–4325.
- Chen, Y., Cao, J.J., Zhao, J., Xu, H.M., Arimoto, R., Wang, G.H., Han, Y.M., Shen, Z.X., Li, G.H., 2014. *n*-Alkanes and polycyclic aromatic hydrocarbons in total suspended particulates from the southeastern Tibetan Plateau: concentrations, seasonal variations, and sources. *Sci. Total Environ.* 470, 9–18.
- Chow, J.C., Watson, J.G., Kuhns, H.D., Etyemezian, V., Lowenthal, D.H., Crow, D.J., Kohl, S.D., Engelbrecht, J.P., Green, M.C., 2004. Source profiles for industrial, mobile, and area sources in the Big Bend Regional Aerosol Visibility and Observational (BRAVO) Study. *Chemosphere* 54, 185–208.
- Chuang, M.T., Lee, C.T., Chou, C.C.K., Lin, N.H., Sheu, G.R., Wang, J.L., Chang, S.C., Wang, S.H., Chi, K.H., Young, C.Y., Huang, H., Chen, H.W., Weng, G.H., Lai, S.Y., Hsu, S.P., Chang, Y.J., Chang, J.H., Wu, X.C., 2014. Carbonaceous aerosols in the air masses transported from Indochina to Taiwan: long-term observation at Mt. Lulin. *Atmos. Environ.* 89 (2), 507–516.
- Cong, Z.Y., Kang, S.C., Kawamura, K., Liu, B., Wan, X., Wang, Z., Gao, S., Fu, P., 2015. Carbonaceous aerosols on the south edge of the Tibetan Plateau: concentrations, seasonality and sources. *Atmos. Chem. Phys.* 15, 1573–1584.
- Crutzen, P.J., Andreae, M.O., 1990. Biomass burning in the tropics: impact on atmospheric chemistry and biogeochemical cycles. *Science* 250, 1669–1678.
- Crutzen, P.J., Heidt, L.E., Krasnec, J.P., Pollock, W.H., Seiler, W., 1979. Biomass burning as a source of atmospheric gases CO, H<sub>2</sub>, N<sub>2</sub>O, NO, CH<sub>3</sub>Cl and COS. *Nature* 282, 253–256.
- Decesari, S., Facchini, M.C., Carbone, C., Giulianelli, L., Rinaldi, M., Finessi, E., Fuzzi, S., Marinoni, A., Cristofanelli, P., Duchi, R., Bonasoni, P., Vuillermoz, E., Cozic, J., Jaffredo, J.L., Laj, P., 2010. Chemical composition of PM<sub>10</sub> and PM<sub>2.5</sub> at the high-altitude Himalayan station Nepal Climate Observatory-Pyramid (NCO-P) (5079 m a.s.l.). *Atmos. Chem. Phys.* 10, 4583–4596.
- Engling, G., Zhang, Y.N., Chan, C.Y., Sang, X.F., Lin, M., Ho, K.F., Li, Y.S., Lin, C.Y., Lee, J.J., 2011. Characterization and sources of aerosol particles over the southeastern Tibetan Plateau during the Southeast Asia biomass-burning season. *Tellus B* 63, 117–128.
- Giglio, L., Randerson, J.T., Werf, G.R.V.D., 2013. Analysis of daily, monthly, and annual burned area using the fourth-generation global fire emissions database (gfd4). *J. Geophys. Res. Biogeosci.* 118 (1), 317–328.
- Gong, P., Wang, X.P., Yao, T.D., 2011. Ambient distribution of particulate- and gas-phase *n*-alkanes and polycyclic aromatic hydrocarbons in the Tibetan Plateau. *Environ. Earth Sci.* 64, 1703–1711.
- Gustafsson, O., Krusa, M., Zencak, Z., Sheesley, R.J., Granat, L., 2009. Brown clouds over South Asia: biomass or fossil fuel combustion? *Science* 323, 495–498.
- Haberle, S.G., Hope, G.S., van der Kaars, S., 2001. Biomass burning in Indonesia and Papua New Guinea: natural and human induced fire events in the fossil record. *Palaeogeogr. Palaeoclimatol. Palaeoecol.* 171 (3–4), 259–268.
- Han, Y.M., Cao, J.J., Chow, J.C., Watson, J.G., Fung, K., Jin, Z.D., Liu, S.X., An, Z.S., 2007. Evaluation of the thermal/optical reflectance method for discrimination between soot- and char-EC. *Chemosphere* 69, 569–574.
- Han, Y.M., Lee, S.C., Cao, J.J., Ho, K.F., An, Z.S., 2009. Spatial distribution and seasonal variation of char-EC and soot-EC in the atmosphere over China. *Atmos. Environ.* 43, 6066–6073.
- Ho, S.S.H., Chow, J.C., Watson, J.G., Ting Ng, L.P., Kwok, Y., Ho, K.F., Cao, J.J., 2011. Precautions for in-injection port thermal desorption-gas chromatography/mass spectrometry (TD-GC/MS) as applied to aerosol filter samples. *Atmos. Environ.* 45, 1491–1496.
- Huang, X.F., He, L.Y., Hu, M., Zhang, Y.H., 2006. Annual variation of particulate organic compounds in PM<sub>2.5</sub> in the urban atmosphere of Beijing. *Atmos. Environ.* 40 (14), 2449–2458.
- Huang, K., Fu, J.S., Hsu, N.C., Gao, Y., Dong, X., Tsay, S.C., 2013. Impact assessment of biomass burning on air quality in Southeast and East Asia during BASE-ASIA. *Atmos. Environ.* 78 (7), 291–302.
- Kaufman, Y.J., Justice, C.O., Flynn, L.P., Kendall, J.D., Prins, E.M., Giglio, L., Ward, D.E., Menzel, W.P., Setzer, A.W., 1998. Potential global fire monitoring from EOS-MODIS. *J. Geophys. Res.* 103, 32215–32238.
- Khamkaew, C., Chantara, S., Janta, R., Pani, S.K., Prapamontol, T., Kawichai, S., et al., 2016. Investigation of biomass burning chemical components over Northern Southeast Asia during 7-SEAS/BASELINE 2014 campaign. *Aerosol Air Qual. Res.* 16 (11), 2655–2670.
- Lee, J.Y., Kim, Y.P., Kaneyasu, N., Kumata, H., Kang, C.H., 2008. Particulate PAHs levels at Mt. Halla site in Jeju Island, Korea: regional background levels in northeast Asia. *Atmos. Res.* 90, 91–98.
- Lin, N.H., Tsay, S.C., Maring, H.B., Yen, M.C., Sheu, G.R., Wang, S.H., et al., 2013. An overview of regional experiments on biomass burning aerosols and related pollutants in Southeast Asia: from BASE-ASIA and the Dongsha experiment to 7-SEAS. *Atmos. Environ.* 78 (78), 1–19.
- Lin, J.C., Matsui Sr., T., P. R.A., Kummerow, C., 2016. Effects of biomass-burning-derived aerosols on precipitation and clouds in the Amazon Basin: a satellite-based empirical study. *J. Geophys. Res. Atmos.* 111 (D19), 4617–4632.
- Liu, J., Li, J., Lin, T., Liu, D., Xu, Y., Chaemfa, C., 2013. Diurnal and nocturnal variations of PAHs in the Lhasa atmosphere, Tibetan Plateau: implication for local sources and the impact of atmospheric degradation processing. *Atmos. Res.* 124, 34–43.
- Ma, Y., Weber, R.J., Lee, Y.N., Orsini, D.A., Maxwell-Meier, K., Thornton, D.C., Bandy, A.R., Clarke, A.D., Blake, D.R., Sachse, G.W., Fuelberg, H.E., Kiley, C.M., Woo, J.H., Streets, D.G., Carmichael, G.R., 2003. Characteristics and influence of biomass on the fine-particle ionic composition measured in Asian outflow during the Transport and Chemical Evolution over the Pacific (TRACE-P) experiment. *J. Geophys. Res.* 108 (D21).
- Ma, W.L., Sun, D.Z., Shen, W.G., Yang, M., Qi, H., Liu, L.Y., 2011. Atmospheric concentrations, sources and gas-particle partitioning of PAHs in Beijing after the 29th Olympic Games. *Environ. Pollut.* 159, 1794–1801.
- Niu, H., Cheng, W., Hu, W., Wei, P., 2016. Characteristics of individual particles in a severe short-period haze episode induced by biomass burning in Beijing. *Atmos. Pollut. Res.* 7 (6), 1072–1081.
- Oliveira, C., Martins, N., Tavares, J., Pio, C., Cerqueira, M., Matos, M., Silva, H., Oliveira, C., Cameses, F., 2011. Size distribution of polycyclic aromatic hydrocarbons in a roadway tunnel in Lisbon, Portugal. *Chemosphere* 83 (11), 1588–1596.

- Ordou, N., Agranovski, I.E., 2017. Mass distribution and elemental analysis of the resultant atmospheric aerosol particles generated in controlled biomass burning processes. *Atmos. Res.* 198, 108–112.
- Pani, S.K., Wang, S., Lin, N., Tsay, S., Lolli, S., Chuang, M., et al., 2016. Assessment of aerosol optical property and radiative effect for the layer decoupling cases over the northern south china sea during the 7-SEAS/Dongsha Experiment. *J. Geophys. Res. Atmos.* 121 (9), 4894–4906.
- Pimonsree, S., Vongruang, P., Sumitsawan, S., 2017. Modified biomass burning emission in modeling system with fire radiative power: simulation of particulate matter in mainland Southeast Asia during smog episode. *Atmos. Pollut. Res.* 9, 133–145.
- Pochanart, P., Akimoto, H., Kajii, Y., Sukasem, P., 2003. Carbon monoxide, regional scale transport, and biomass burning in tropical continental Southeast Asia: observations in rural Thailand. *J. Geophys. Res.* 108 (D17), 4552.
- Radojevic, M., 2003. Chemistry of forest fires and regional haze with emphasis on Southeast Asia. *Pure Appl. Geophys.* 160 (1–2), 157–187.
- Ram, K., Sarin, M.M., 2010. Spatio-temporal variability in atmospheric abundances of EC, OC and WSOC over northern India. *J. Aerosol Sci.* 41, 88–98.
- Ramanathan, V., Ramana, M.V., Roberts, G., Kim, D., Corrigan, C., 2007. Warming trends in Asia amplified by brown cloud solar absorption. *Nature* 448, 575–578.
- Ravindra, K., Sokhi, R., Van Grieken, R., 2008. Atmospheric polycyclic aromatic hydrocarbons: source attribution, emission factors and regulation. *Atmos. Environ.* 42, 2895–2921.
- Reid, J.S., Koppmann, R., Eck, T.F., Eleuterio, D.P., 2005. A review of biomass burning emissions part III: intensive optical properties of biomass burning particles. *Atmos. Chem. Phys.* 4 (5), 827–849.
- Rissanen, T., Hyötyläinen, T., Kallio, M., Kronholm, J., Kulmala, M., Riekkola, M.L., 2006. Characterization of organic compounds in aerosol particles from a coniferous forest by GC-MS. *Chemosphere* 64, 1185–1195.
- Salam, A., Bauer, H., Kassim, K., Ullah, S.M., Puxbaum, H., 2003. Aerosol chemical characteristics of a mega-city in Southeast Asia (Dhaka–Bangladesh). *Atmos. Environ.* 37, 2517–2528.
- Sánchez, d.I.C.A.M., Salvador, P., Fernándezcamacho, R., Artiñano, B., Coz, E., Márquez, G., 2018. Characterization of biomass burning from olive grove areas: a major source of organic aerosol in PM<sub>10</sub> of Southwest Europe. *Atmos. Res.* 199, 1–13.
- Sang, X.F., Zhang, Z.S., Chan, C.Y., Engling, G., 2013. Source categories and contribution of biomass smoke to organic aerosol over the southeastern Tibetan Plateau. *Atmos. Environ.* 78, 113–123.
- Sayer, A.M., Hsu, N.C., Hsiao, T.C., Pantina, P., Kuo, F., Ou-Yang, C.F., et al., 2016. In-situ and remotely-sensed observations of biomass burning aerosols at Doi Ang Khang, Thailand during 7-SEAS/BASELInE 2015. *Aerosol Air Qual. Res.* 16, 2786–2801.
- Schultz, M.G., 2002. On the use of ATSR fire count data to estimate the seasonal and interannual variability of vegetation fire emissions. *Atmos. Chem. Phys.* 2, 387–395.
- Sheesley, R.J., Schauer, J.J., Chowdhury, Z., Cass, G.R., Simoneit, B.R.T., 2003. Characterization of organic aerosols emitted from the combustion of biomass indigenous to South Asia. *J. Geophys. Res.* 108 (D9), 1761–1762.
- Shen, Z.X., Cao, J.J., Arimoto, R., Han, Z.W., Zhang, R.J., Han, Y.M., Liu, S.X., Okuda, T., Nakao, S., Tanaka, S., 2009. Ionic composition of TSP and PM<sub>2.5</sub> during dust storms and air pollution episodes at Xi'an, China. *Atmos. Environ.* 43, 2911–2918.
- Soja, A.J., Al-Saadi, J., Giglio, L., et al., 2009. Assessing satellite-based fire data for use in the National Emission Inventory. *J. Appl. Remote. Sens.* 3 (1), 031504–031504-29.
- Souza, M.L., Allen, A.G., Cardoso, A.A., 2016. Understanding aerosol formation mechanisms in a subtropical atmosphere impacted by biomass burning and agroindustry. *Atmos. Res.* 183, 94–103.
- Stohl, A., Forster, C., Huntrieser, H., Mannstein, H., McMillan, W.W., Petzold, A., Schlager, H., Weinzierl, B., 2007. Aircraft measurements over Europe of an air pollution plume from Southeast Asia - aerosol and chemical characterization. *Atmos. Chem. Phys.* 7, 913–937.
- Stone, E.A., Lough, G.C., Schauer, J.J., Praveen, P.S., Corrigan, C.E., 2007. Understanding the origin of black carbon in the atmospheric brown cloud over the Indian Ocean. *J. Geophys. Res.* 112 (D22S23), 365–371.
- Tian, J., Ni, H.Y., Cao, J.J., Han, Y.M., Wang, Q.Y., Wang, X.L., et al., 2017. Characteristics of carbonaceous particles from residential coal combustion and agricultural biomass burning in China. *Atmos. Pollut. Res.* 8 (3), 521–527.
- Tsay, S.C., Maring, H.B., Lin, N.H., Buntoung, S., Chantara, S., Chuang, H.C., et al., 2016. Satellite-surface perspectives of air quality and aerosol-cloud effects on the environment: an overview of 7-SEAS/BASELInE. *Aerosol Air Qual. Res.* 16 (11), 2581–2602.
- Venkataraman, C., Habib, G., Eiguren-Fernandez, A., Miguel, A.H., Friedlander, S.K., 2005. Residential biofuels in south Asia: carbonaceous aerosol emissions and climate impacts. *Science* 307 (5714), 1454–1456.
- Vicente, E.D., Alves, C.A., 2017. An overview of particulate emissions from residential biomass combustion. *Atmos. Res.* 199, 159–185.
- Wang, S.H., Lin, N.H., Chou, M.D., Woo, J.H., 2007. Estimate of radiative forcing of Asian biomass-burning aerosols during the period of TRACE-P. *J. Geophys. Res.* 112, D10222.
- Wang, S.H., Welton, E.J., Holben, B.N., Tsay, S.C., Lin, N.H., Giles, D., et al., 2015. Vertical distribution and columnar optical properties of springtime biomass-burning aerosols over northern Indochina during 2014 7-SEAS campaign. *Aerosol Air Qual. Res.* 15 (5), 2037–2050.
- Wingfors, H., Hägglund, L., Magnusson, R., 2011. Characterization of the size-distribution of aerosols and particle-bound content of oxygenated PAHs, PAHs, and n-alkanes in urban environments in Afghanistan. *Atmos. Environ.* 45, 4360–4369.
- Xu, J.Z., Zhang, Q., Wang, Z.B., Yu, G.M., Ge, X.L., Qin, X., 2015. Chemical composition and size distribution of summertime PM<sub>2.5</sub> at a high altitude remote location in the northeast of the Qinghai-Xizang (Tibet) Plateau: insights into aerosol sources and processing in free troposphere. *Atmos. Chem. Phys.* 15, 5069–5081.
- Yadav, I.C., Linthoingambi, D.N., Li, J., Syed, J.H., Zhang, G., Watanabe, H., 2017. Biomass burning in Indo-China peninsula and its impacts on regional air quality and global climate change-a review. *Environ. Pollut.* 227, 414–427.
- Yunker, M.B., Macdonald, R.W., Vingarzan, R., Mitchell, R.H., Goyette, D., Sylvestre, S., 2002. PAHs in the Fraser River basin: a critical appraisal of PAH ratios as indicators of PAH source and composition. *Org. Geochem.* 33, 489–515.
- Zeng, T., Wang, Y., Yoshida, Y., Tian, D., Russell, A.G., Barnard, W.R., 2008. Impacts of prescribed fires on air quality over the southeastern United States in spring based on modeling and ground/satellite measurements. *Environ. Sci. Technol.* 42 (22), 8401–8406.
- Zeng, T., Liu, Z., Wang, Y.H., 2016. Large fire emissions in summer over the southeastern US: satellite measurements and modeling analysis. *Atmos. Environ.* 127, 213–220.
- Zhang, X., Hecobian, A., Zheng, M., Frank, N.H., Weber, R.J., 2010. Biomass burning impact on PM<sub>2.5</sub> over the southeastern US during 2007: integrating chemically speciated FRM filter measurements, MODIS fire counts and PMF analysis. *Atmos. Chem. Phys.* 10, 6839–6853.
- Zhang, N.N., Cao, J.J., Liu, S.X., Zhao, Z.Z., Xu, H.M., Xiao, S., 2014. Chemical composition and sources of PM<sub>2.5</sub> and TSP collected at Qinghai Lake during summertime. *Atmos. Res.* 138, 213–222.
- Zhang, N.N., Cao, J.J., Huang, R.J., He, Y.Q., Wang, Q.Y., Zhu, C.S., 2016. Seasonal variation, sources and transport of aerosols at Lijiang, Southeast Tibetan Plateau. *Aerosol Air Qual. Res.* 16 (7), 1579–1590.
- Zhao, Z.Z., Cao, J.J., Shen, Z.X., Xu, B.Q., Zhu, C.S., Chen, L.-W.A., Su, X.L., Han, Y.M., Wang, G.H., Ho, K.F., 2013. Aerosol particles at a high-altitude site on the Southeast Tibetan Plateau, China: implications for pollution transport from South Asia. *J. Geophys. Res.* 118, 11360–11375.
- Zheng, J., Hu, M., Du, Z., Shang, D., Gong, Z., Qin, Y., Fang, J., Gu, F., Li, M., Peng, J., Li, J., Zhang, Y., Huang, X., He, L., Wu, Y., Guo, S., 2017. Influence of biomass burning from Southeast Asia at a high-altitude mountain receptor site in China. 2017. *Atmos. Chem. Phys.* 17, 6853–6864.
- Zhu, C.S., Cao, J.J., Tsai, C.J., Zhang, Z.S., Tao, J., 2017a. Biomass burning tracers in rural and urban ultrafine particles in Xi'an, China. *Atmos. Pollut. Res.* 8 (4), 614–618.
- Zhu, J., Xia, X.A., Wang, J., Zhang, J.Q., Wiedinmyer, C., Fisher, J.A., Keller, C.A., 2017b. Impact of Southeast Asian smoke on aerosol properties in Southwest China: first comparison of model simulations with satellite and ground observation. *J. Geophys. Res.* 122. <http://dx.doi.org/10.1002/2016JD025793>.